# Modeling formation and subsequent nonlinear evolution of rip channels: Time-varying versus time-invariant wave forcing

B. Castelle[1] and B. G. Ruessink[2]

[1] We use a nonlinear morphodynamic model to demonstrate that time-varying forcing, in particular the time-varying angle of wave incidence, is crucial to the development of rip channels in terms of rip channel morphology, nonlinear behavior, longshore migration, and mean rip spacing. The time-varying angle of incidence leads to different mean rip spacings than the time-integrated time-invariant forcing and to systematically less developed bar and rip morphologies at more alongshore variable scales. This supports the common field observation of irregular and random alongshore rip spacings, and contrasts with the regular spacing predicted by existing time-invariant template, and instability models. Time-varying wave incidence also generally results in the onset of splitting of shoals and an increase in merging of rip channels. In addition, a time-varying angle of incidence with zero mean can drive a significant net alongshore migration of the rip channels. Abrupt changes in wave conditions are responsible for this net longshore migration through cumulative effects of the mismatch between wave conditions and bar and rip morphology orientation.

**Citation:** Castelle, B., and B. G. Ruessink (2011), Modeling formation and subsequent nonlinear evolution of rip channels: Time-varying versus time-invariant wave forcing, *J. Geophys. Res.*, *116*, F04008, doi:10.1029/2011JF001997.

## 1. Introduction

[2] Rip channels are ubiquitous and striking patterns in the sand along wave-dominated beaches. They are important from the perspective of localized beach and dune erosion as well as beach safety and mixing in the nearshore. Rip channels are often part of an accretionary, down-state sequence developing from an alongshore-uniform barred-beach state [*Wright and Short*, 1984] following a storm event. During this extended period of beach recovery, shoals develop from the shallowest sections of the alongshore bar that progressively migrate onshore and in some cases they can even attach to the beach [*Van Enckevort et al.*, 2004]. Depending on the dominant wave-angle to the shore, rip channels can be shore-normal to strongly skewed downdrift [*Wright and Short*, 1984]. During severe storms, or during moderate-energy waves with high angle of incidence [*Price and Ruessink*, 2011], rip channels are reshaped into an alongshore-uniform feature [*Van Enckevort et al.*, 2004], often with concurrent erosion of the beach face.

[3] The emergence and dynamics of rip channels have puzzled scientists for decades. *Coco and Murray* [2007] reviewed the shift from (edge-wave) forcing template to self-organization theories for explaining the formation and subsequent nonlinear evolution of rip channels. Using self-organization models, it was established that rip channels and other three-dimensional (3-D) sandbar patterns, such as crescentic sandbars, form through the positive feedback between flow (waves and currents), sediment processes, and the evolving seabed morphology and that their formation does not require a template in the hydrodynamics.

[4] Linear stability models [*Deigaard et al.*, 1999; *Falqués et al.*, 2000; *Calvete et al.*, 2005; *Klein and Schuttelaars*, 2006], restricted to the initial development of the 3-D patterns using a number of simplifying assumptions, predict rip channels with similar alongshore scales to those observed in the field, with larger length scales for oblique incidence waves. Most importantly, these models allowed both identification of the physical mechanisms that govern feedbacks leading to self-organization [*Falqués et al.*, 2000; *Ribas and Kroon*, 2007] and examination of the role of different parameters such as wave height, period, and direction [*Damgaard et al.*, 2002; *Calvete et al.*, 2007] on characteristic length and timescales. Recently, nonlinear models [e.g., *Damgaard et al.*, 2002; *Reniers et al.*, 2004; *Castelle et al.*, 2006a; *Drønen and Deigaard*, 2007; *Garnier et al.*, 2008; *Smit et al.*, 2008] have been developed to examine the initial growth and subsequent nonlinear evolution of rip channels and crescentic planshapes. Nonlinear morphodynamic models allow temporal changes in the wavelength and the amplitude of the 3-D patterns to be examined.

[5] The recent growing number of high-frequency field observations of sandbar evolution through video imagery has improved our knowledge of rip channel behavior along wave-dominated sandy beaches [e.g., *Van Enckevort and Ruessink*, 2003; *Holman et al.*, 2006; *Turner et al.*, 2007;

[1]CNRS, UMR 5805 EPOC, Université de Bordeaux, Talence, France.
[2]Department of Physical Geography, Faculty of Geosciences, Institute for Marine and Atmospheric Research, Utrecht University, Utrecht, Netherlands.

*Ruessink et al.*, 2007a; *Almar et al.*, 2010; *Price and Ruessink*, 2011; *Gallop et al.*, 2011]. Some studies have tried to identify potential relationships between rip channel wavelength and the prevailing offshore wave conditions [*Huntley and Short*, 1992; *Holman et al.*, 2006; *Turner et al.*, 2007]. Surprisingly, all these studies found poor correlation between rip spacing and wave conditions. Three major arguments can be put forward to explain this lack of correlation. First, rip wavelength may become morphologically controlled soon after a storm reset event [*Turner et al.*, 2007] and is thus unrelated to subsequent variations in offshore wave conditions. Second, rip-channel evolution with time may be much slower than typical timescales associated with changes in offshore wave conditions. In particular, rip channels with a long cross-shore length and wide alongshore spacing have been observed to respond slower to changes in wave conditions than rips with a short cross-shore length and narrower alongshore spacing [*Gallop et al.*, 2011]. Third, rip channel wavelength sensitivity to the initial cross-shore profile is high, implying that the underlying bathymetry is as crucial as wave conditions to the development of rip channels [*Calvete et al.*, 2007].

[6] Because linear stability analysis is restricted to the initial growth of rip channels, time-invariant forcing is an appropriate condition under which to undertake such a modeling exercise. Only *Tiessen et al.* [2010] addressed time-varying wave conditions to show that combining linear stability analysis with an appropriate algorithm which identifies the more physically representative model results resulted in a fair agreement of predicted length scales of the crescentic bed patterns with observations. Surprisingly, all existing nonlinear morphodynamic modeling studies use time-invariant wave forcing, with only two exceptions. First, *Smit et al.* [2005] investigated the dynamics of a double sandbar system to changes in wave conditions. They noted both the important role of the antecedent morphology and that the bathymetry evolved in a similar way for the time-invariant conditions as for rapidly varying wave conditions. This study was limited to a small number of simulations and was further complicated by the feedbacks between the two sandbar systems. Second, *Reniers et al.* [2004] addressed time-varying conditions at the timescales of wave groups ($O(100 \text{ s})$), which is different from addressing time-varying forcing at the change in wave regime timescales ($O(1–10 \text{ days})$). The assumption of time-invariant forcing suggests that rip channel evolution time is shorter than natural variability in the forcing [see, e.g., *Turner et al.*, 2007]. Consequently, all the nonlinear morphodynamic modeling studies to date (except *Smit et al.* [2005]) investigated rip channel evolution as if the wave climate is constant, incompatible with the persistent changes in natural wave conditions. Accordingly, the impact of time-varying wave conditions on finite-amplitude rip channel dynamics remains poorly understood.

[7] In this paper we use a nonlinear morphodynamic model (section 2) to compare predictions of nonlinear rip channel evolution under time-invariant (section 3) and time-varying (section 4) wave forcing and demonstrate that, in particular, a time-varying angle of incidence results in substantially different predictions from those for a time-

invariant angle. The discussion and conclusions are presented in section 5.

## 2. Nonlinear Morphodynamic Model

### 2.1. Set of Equations

[8] We used a nonlinear morphodynamic model [*Castelle et al.*, 2010a, 2010b] that couples a spectral wave model, a time- and depth-averaged flow model, an energetics-type sediment transport model, and the bed level continuity equation to compute bed level changes. The wavefield and resulting radiation stress components are computed from the spectral wave model SWAN [*Booij et al.*, 1999], which solves the spectral wave-action balance, here with default parameter settings.

[9] The flow model is based on the phase-averaged nonlinear shallow water equations comprising the water mass conservation and momentum conservation equations:

$$\frac{\partial Q_i}{\partial t} + \frac{\partial}{\partial x_j}\left(\frac{Q_i Q_j}{h}\right) = -gh\frac{\partial \eta}{\partial x_i} - \frac{1}{\rho}\frac{\partial S_{ij}}{\partial x_j} + \frac{1}{\rho}\frac{\partial T_{ij}}{\partial x_j} - \frac{\tau_i^b}{\rho} \quad (1)$$

$$\frac{\partial \eta}{\partial t} + \frac{\partial Q_j}{\partial x_j} = 0 \quad (2)$$

where $h$ is the mean water depth; $Q_i$ are the water volume fluxes, with the subscript $i$ referring to the two horizontal coordinates (with $x$ and $y$ the alongshore and cross-shore axis, respectively); $\eta$ is the mean free surface elevation; $g$ is the gravitational acceleration; $\rho$ is the water density; $S_{ij}$ are the radiation stress components [*Phillips*, 1977]; $\tau_i^b$ is the bed shear stress; and $T_{ij}$ is the lateral shear stress which is the horizontal momentum exchange due to the combined action of turbulence and the mean current using the formulation proposed by *Battjes* [1975]. More details on the flow model and the validation with field data are given by *Castelle et al.* [2006b].

[10] In the work of *Castelle et al.* [2010a] the combined bed and suspended load sediment transport $\vec{Q}_s$ was computed using the formulations of *Bailard* [1981], using default settings. This approach cannot be used if one wants to run simulations over long durations, i.e., several times the typical growth time, as the model would blow up when the bar amplitude becomes too large compared to that in nature. Therefore we modified the original code to examine the finite amplitude dynamics through an adequate treatment of the gravitational downslope sediment transport, as in the work of *Garnier et al.* [2008]. In our model the horizontal sediment flux vector $\vec{Q}_s$ is

$$\vec{Q}_s = \alpha\left(\overline{|\vec{u}_b(t)|^3 \vec{u}_b(t)} - \gamma u_{rms}\vec{\nabla}Z\right) \quad (3)$$

where $\alpha$ is a stirring factor; $\gamma$ is a bed slope coefficient; $u_{rms}$ is the root mean square wave orbital velocity amplitude at the bottom; $\vec{u}_b(t)$ is the total instantaneous flow velocity at the bottom (mean currents and orbital velocity) with the notation $\overline{()}$ indicating the time-averaging over a duration larger than the typical wave period and $Z$ is the bed level deviation from initial equilibrium, such that $Z = Z_f - Z_f^0$ where $Z_f^0$ is the initial bed level, i.e., the basic state. The first

term in equation (3) is similar to the suspended sediment load in the work of *Bailard* [1981] while the second term is the downslope sediment transport with respect to the basic state. First, we set $\alpha$ for $\gamma = 0$ to obtain similar rip channel growth time as in existing modeling studies [e.g., *Garnier et al.*, 2006]. Second, we set $\gamma$ balancing the desire to both prevent any model blow-up in the range of wave conditions used in this study (by increasing $\gamma$) and to have a morphodynamic model as nonlinear as possible (by decreasing $\gamma$). The latter means increasing the possibility of observing splitting and merging dynamics. In the following we set $\alpha = 2.10^{-4} \ \mathrm{s^3.m^{-2}}$ and $\gamma = 100 \ \mathrm{m^2.s^{-1}}$ based on these preliminary tests. Because the advective part in our sediment transport formula $\alpha \, |\vec{u}_b(t)|^3 \vec{u}_b(t)$ is different from that in the work of *Garnier et al.* [2006, 2008, 2010] that reads $\alpha \vec{Q}/h$, our reference values of $\gamma$ and $\alpha$ are not comparable with those in the work of *Garnier et al.* [2006]. Yet, simulated rip channel systems and wave-driven circulations at saturation are similar in patterns.

[11] The new seabed level $Z_f$ was computed using the sediment mass conservation equation:

$$\frac{\partial Z_f}{\partial t} + \frac{1}{1-p} \vec{\nabla} \vec{Q}_s = 0 \qquad (4)$$

where $p = 0.4$ is the sediment porosity. The morphological time step for the bed update scheme was 1 h throughout. All the simulations were run for 996 morphological time steps, that is, 41.5 days of morphological evolution. Note that the shoreline is allowed to evolve. This represents a major difference with other nonlinear morphodynamic models applied to 3-D surfzone sandbar behavior.

## 2.2. Model Setup

[12] We ran the model for one initial single-barred beach geometry. This choice of a single bar setting was motivated by recent studies unraveling the highly complex behavior of inner-bar rip channel systems in multiple-barred settings due to morphological feedbacks between the sandbars [*Masselink et al.*, 2006; *Ruessink et al.*, 2007a; *Castelle et al.*, 2010a, 2010b; *Almar et al.*, 2010; *Price and Ruessink*, 2011]. A single-barred beach setting prevents such complexity. The computational grid had an alongshore length of 5000 m, 20 × 20 m grid cells, and periodic lateral boundary conditions. Additional simulations with a larger domain showed that these periodic boundary conditions did not significantly affect rip channel behavior. About 10 rip channels were typically observed in the 5000-m long domain. This number of simulated rip channels is similar to existing modeling studies of rip channel and crescentic bar with periodic lateral boundaries [e.g., *Garnier et al.*, 2008].

[13] The basic state consisted of a beach with a 1:50 planar sloping depth profile, with its offshore extent in 10.6 m water depth. A bar was superimposed on this planar profile, located 90 m from the mean sea level shoreline at $y = 140$ m with its crest in 0.8 m depth. This choice of bar geometry was motivated by the aim of having a large number of wavelengths in the domain (hence the relatively short distance of the bar crest to the shoreline) and persistent wave breaking across the bar for a range of offshore significant wave heights around 1 m (hence the small water depth at the bar crest). Random perturbations with a magnitude of 1 mm in the seabed were superimposed on the initial alongshore-uniform single-barred beach to excite nearshore instabilities. The initial beach profile together with the cross-shore wave height profiles for $H_s = 0.8$ m, 1 m, and 1.2 m, a peak wave period $T_p = 10$ s and shore-normal wave incidence are shown in Figure 1. These simulations show that the wave height at the bar systematically saturates as a result of intense depth-induced breaking dissipation. According to *Calvete et al.* [2005], this suggests that there will be little dependence of rip spacing on offshore wave height for 0.8 m < $H_s$ < 1.2 m as rip spacing typically increases with offshore wave height up to a saturation value that is reached when the wave height at the bar saturates.

[14] We defined a reference time-invariant wave forcing simulation characterized by $H_s = 1$ m, $T_p = 10$ s and $\theta = 0°$. Additional time-invariant simulations were done with 6 s < $T_p$ < 14 s and 0.8 m < $H_s$ < 1.2 m. This narrow range of $H_s$ values was motivated by the basic state approach in the sediment transport $\vec{Q}_s$ computation. This approach assumes that for the alongshore-uniform basic state, cross-shore sediment transport driven by undertow and wave non-linearities are in balance for the given reference wave conditions. Given natural variability in the wave forcing, the true equilibrium is never reached in the field [*Pape et al.*, 2010]. Therefore when addressing the formation and non-linear evolution of rip channels, we assume that rip channels form and evolve more rapidly than the rate at which the beach profile is changing. On the one hand, weakly to nonbreaking wave conditions result in significant onshore sandbar migration together with a typically slow 3-D pattern development. On the other hand, large waves result in significant ($O(10$ m/day)) offshore sandbar migration, sometimes with reshaping of the 3-D patterns into an alongshore-uniform feature. Accordingly, to be consistent with the assumption that rip channels evolve more rapidly than the rate at which the beach profile is changing, both low and large $H_s$ values were disregarded and a narrow range of wave height values (0.8 m < $H_s$ < 1.2 m), corresponding to the saturated basic states in Figure 1, was considered for both time-invariant and time-varying forcing simulations.

[15] Time-varying wave conditions started after 4 days of time-invariant reference forcing ($H_s = 1$ m, $T_p = 10$ s and $\theta = 0°$). This choice will be discussed in section 5. For a given wave parameter ($H_s$, $T_p$ or $\theta$), the time-varying forcing was defined by an amplitude $A$ (0.1 and 0.2 m for $H_s$; 1, 2, 3, and 4 s for $T_p$; 2, 4, 6, and 8° for $\theta$), a period $T$ (2, 4, 8, and 16 days), and a shape. Four shapes were addressed (Figure 2): sine wave, sawtooth, sawtooth-sine wave, and block function, all with a mean corresponding to the time-invariant reference forcing.

## 2.3. Rip Channel Evolution

[16] To examine the evolution of the single-barred beach, we computed a number of parameters representative of the morphological evolution. First, we computed at every time step the alongshore beach profile located at $y = 100$ m between the bar crest and the mean-sea level shoreline denoted $Z_f(x,100,t)$ to estimate rip channel time evolution. Fourier analysis of the time evolution of this alongshore profile, i.e., local analysis, has been commonly used to compute the predominant rip spacing when modeling the
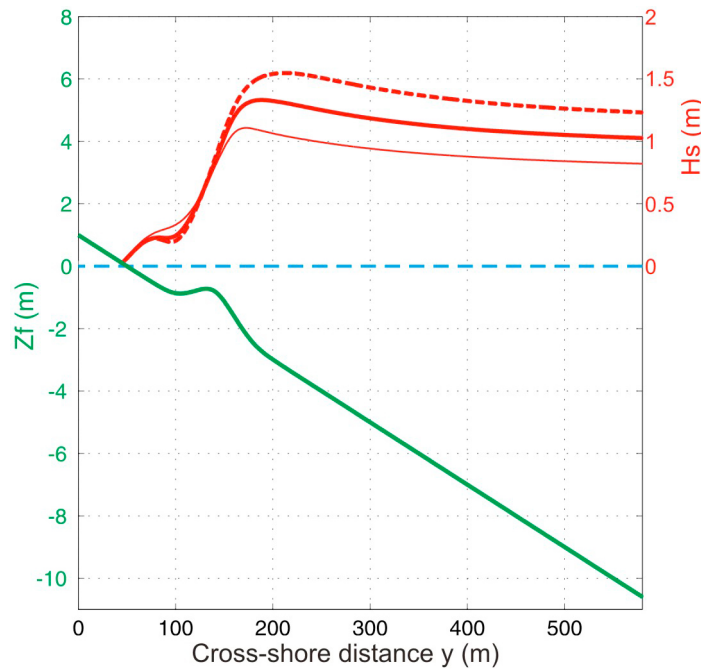
**Figure 1.** Initial beach profile (basic state) used for all the simulations with cross-shore evolution of the significant wave height profile for $H_s = 0.8$ m (thin red line), $H_s = 1$ m (thick solid red line), and $H_s = 1.2$ m (thick dashed red line). The three simulations show a saturated basic state situation because of intense wave energy dissipation through depth-induced breaking across the bar.

formation and evolution of rip channels [e.g., *Garnier et al.*, 2008]. Here, because in our time-varying simulations rip channels often exhibited significant variability in the alongshore scales and depths, this approach was not suitable. Instead we manually counted the number of rip channels to estimate mean rip spacing $\lambda$.

[17] In addition, we used a global analysis of beach evolution [*Garnier et al.*, 2006, 2010] which consists of analyzing variables that are integrated over the whole computational domain. Accordingly, we introduce the overbar notation $\overline{()}$ to define an average over the computational domain, which reads, for a given function $f = f(x, y, t)$:

$$\bar{f}(t) = \frac{1}{L_x L_y} \int_0^{L_x} \int_0^{L_y} f(x, y, t) dx dy \qquad (5)$$

where $L_x$ and $L_y$ are the longshore and cross-shore length of the computational domain, respectively. By using the same definition as in the work of *Vis-Star et al.* [2008]

and *Garnier et al.* [2010] the global growth rate $\sigma$ is given by

$$\sigma(t) = \frac{1}{2E_z(t)^2} \frac{dE_z(t)^2}{dt} \qquad (6)$$

where $E_z$ reads

$$E_z(t) = \sqrt{\overline{Z(x, y, t)^2}} \qquad (7)$$

so that $E_z^2$ can be considered as the potential energy density of the bedforms [*Vis-Star et al.*, 2008; *Garnier et al.*, 2010].

## 3. Time-Invariant Forcing Simulation

### 3.1. Reference Time-Invariant Simulation

[18] Figure 3 shows the final beach morphology for the reference time-invariant simulation with $H_s = 1$ m, $T_p = 10$ s
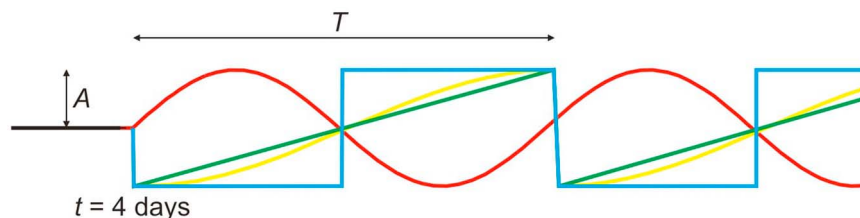


**Figure 2.** Schematic of time-varying wave forcing starting after 4 days of time-invariant reference forcing with an amplitude $A$, a period $T$, and a shape: sine wave (red), sawtooth-sine wave (yellow), sawtooth (green), and block function (blue).
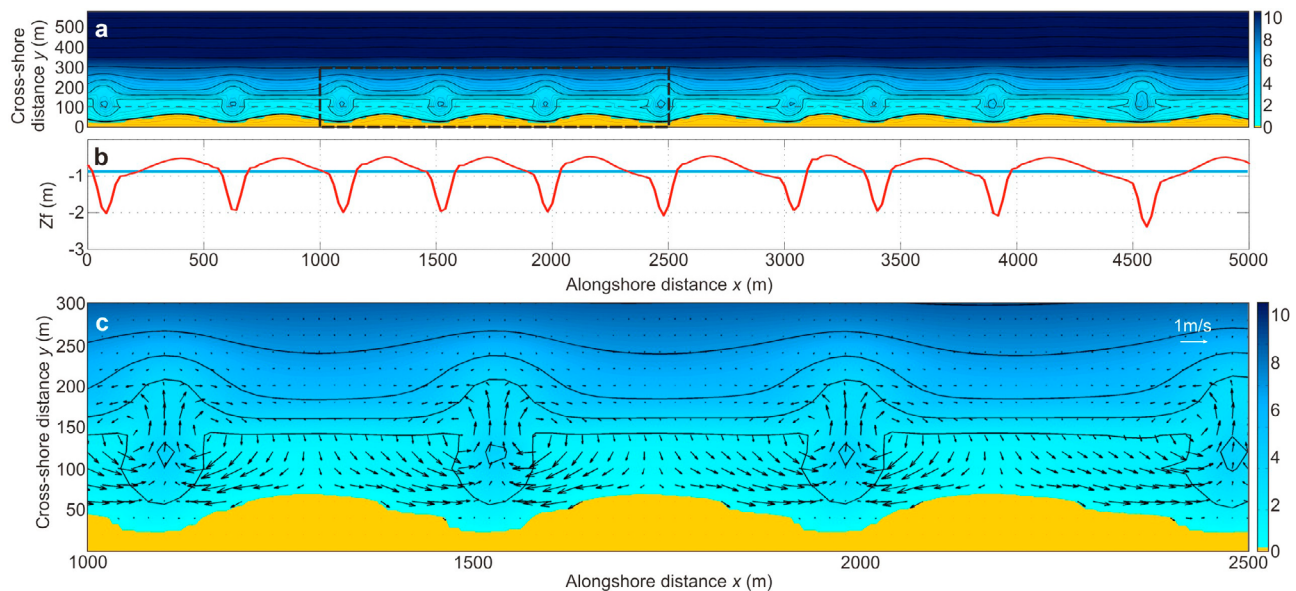
**Figure 3.** (a) Single barred-beach morphology after 41.5 days of simulation (reference time-invariant wave conditions) for time-invariant forcing with $H_s = 1$ m, $T_p = 10$ s, and $\theta = 0°$ together with (b) the alongshore line at $y = 100$ m (dotted gray line) along which bed profile $Z_f(x,100,0)$ and $Z_f(x,100,41.5)$ are given in blue and red, respectively. (c) Zoom of the bathymetry at 1000 m < x < 2500 m and 0 m < y < 300 m with superimposed wave-induced currents. In Figures 3a and 3c the local bottom morphology is contoured in the background and the color bars indicate water depth in meters.

and $\theta = 0°$ at $t = 41.5$ days. The beach exhibits well-developed rip channels at a reasonably narrow range of wavelengths, with a mean $\lambda \approx 500$ m (Figure 3a). All the rip channels show a similar shape with a deep and narrow shore-normal neck and a well-developed rip head bar. The alongshore bed level at $y = 100$ m shows that rip channels are about 1.5 m deep and reasonably narrow with a width of about 50 m (Figure 3b). A zoom on the bathymetry at 1000 m < x < 2500 m, 0 m < y < 300 m with superimposed wave-induced currents is given in Figure 3c. Flow patterns show classic rip current circulations with alongshore feeder currents, reasonably intense and narrow offshore-directed jets in the channel of about 0.5 m/s, strong onshore flows across the shoals and counterrotating cells to the left and the right of the rip current. Because the shoreline is allowed to evolve in our model, erosive features of the rip currents, i.e., megacusps, are clearly present on the beach face, with a cross-shore amplitude of about 40 m. Note that these rip-channel morphologies and wave-driven hydrodynamics are essentially similar to field and laboratory observations of well-developed bar and rip systems exposed to shore-normal low-energy waves [e.g., *Bruneau et al.*, 2009; *Castelle et al.*, 2010c].

[19] Figure 4 shows the time series of $Z_f(x, 100, t)$, $E_z$ and $\sigma$ for the same simulation. The bars appear at day 2–3 (Figure 4a) as $E_z$ starts to be nonzero (Figure 4b). From about day 2–3 to day 5, an initial mode seems to dominate with a mean wavelength $\lambda \approx 350$ m (Figure 4a) with concurrent strongly and linearly increasing $E_z$ (Figure 4b). This corresponds to the linear regime. From day 5 to day 10 rips merge with concurrent less rapidly increasing $E_z$. For instance, at day 7 two clear mergings occur at $x = 2400$ m and $x = 3900$ m. The same applies at day 8 at $x = 200$ m.

From day 10 to the end of the simulation, the predominant wavelength $\lambda \approx 500$ m stabilizes. At day 15 we can consider that the bars have reached a quasi-equilibrium state as bars reached their maximum amplitude. Note that there are no splitting of rip channels throughout this simulation.

### 3.2. Influence of Time-Invariant $H_s$, $T_p$, and $\theta$

[20] We ran a number of simulations to address the influence of $H_s$ and $T_p$ for the given basic state. Simulations show that both $H_s$ and $T_p$ have an influence on the global growth rate as $\sigma$ increases with increasing $H_s$ and increasing $T_p$. Both $H_s$ and $T_p$ also have a significant influence on rip channel morphology. Rip channel depth and width increase and decrease, respectively, with increasing $H_s$ and $T_p$. This is illustrated in Figure 5, which shows examples of time series of $Z_f(x,100,t)$ for different $H_s$ and $T_p$. For shore-normal waves with $T_p = 10$ s and $H_s = 0.8$ m rip channels are less well developed (Figure 3b) than for $H_s = 1.2$ m (Figure 5b, rip channel depth $\approx 2$ m).

[21] The same applies for $T_p$, because for shore-normal waves with $H_s = 1$ m and $T_p = 6$ s (Figure 5c, rip channel depth <0.8 m) rip channels are less developed than for $T_p = 14$ s (Figure 5d, rip channel depth $\approx 1.5$ m). Not surprisingly, $H_s$ has no significant influence on mean rip spacing $\lambda$ because of the saturated basic state for 0.8 m < $H_s$ < 1.2 m (Figure 1), which agrees with *Calvete et al.* [2005]. This is slightly different for $T_p$ as $\lambda$ typically weakly increases with wave period for shore-normal waves according to *Calvete et al.* [2005]. This is apparent in our simulations as nine rip channels are observed for $T_p = 14$ s (Figure 5d) instead of 10 rip channels for both $T_p = 6$ s (Figure 5c) and $T_p = 10$ s (Figure 4a).
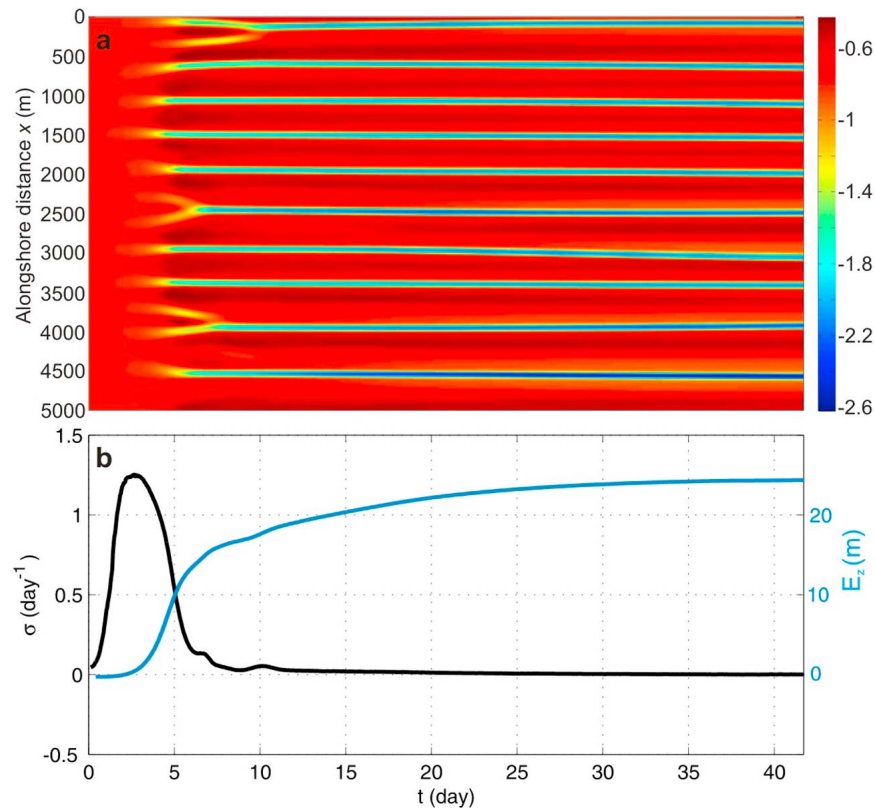
**Figure 4.** Reference time-invariant simulation with (a) time evolution of the alongshore profile $Z_f$ $(x,100,t)$ with corresponding time series of (b) global growth rate $\sigma$ and potential energy density of the bedforms $E_z$.
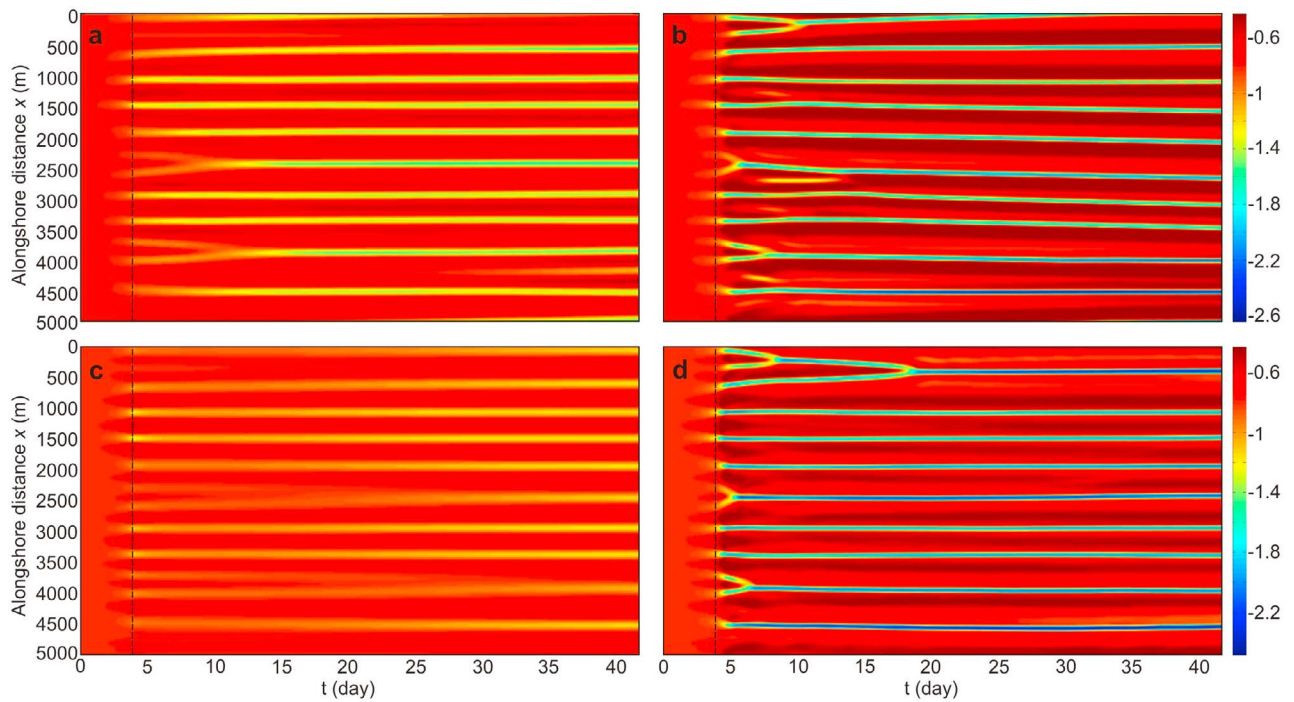
**Figure 5.** Time evolution of the alongshore profile $Z_f(x,100,t)$, starting at $t = 0$ with $H_s = 1$ m, $T_p = 10$ s and $\theta = 0°$, with changing significant wave height $H_s$ at $t = 4$ days with (a) $H_s = 0.8$ m and (b) $H_s = 1.2$ m, and changing peak wave period $T_p$ at $t = 4$ days with (c) $T_p = 6$ s, and (d) $T_p = 14$ s. Color bars indicate seabed elevation in meters.
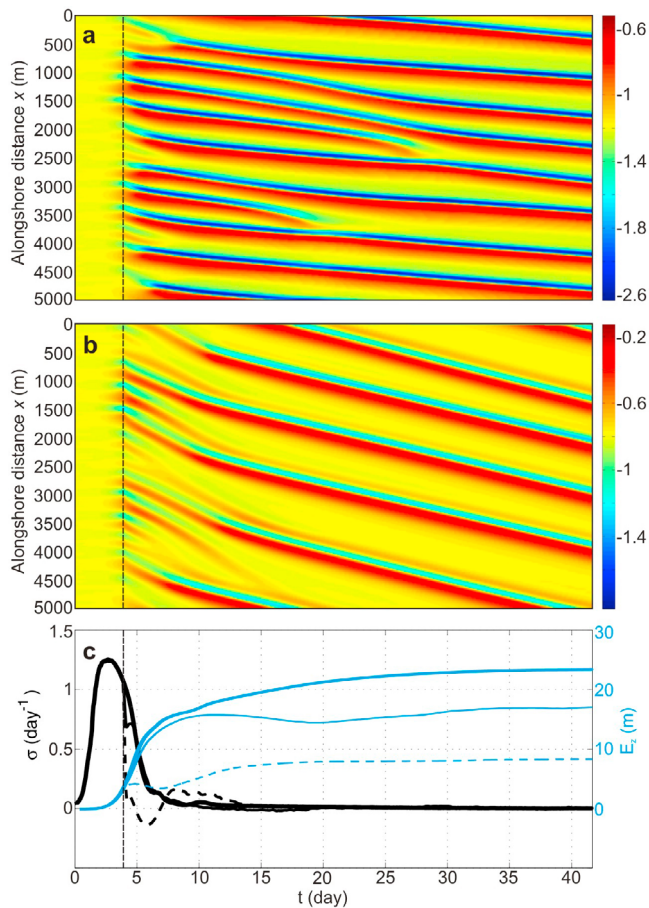
**Figure 6.** Time evolution of the alongshore profile $Z_f$ $(x,100,t)$, starting at $t = 0$ with $H_s = 1$ m, $T_p = 10$ s and $\theta = 0°$, and changing wave angle to the shore at $t = 4$ days with (a) $\theta = 2°$ and (b) $\theta = 4°$, the color bars indicate seabed elevation in meters. (c) Global growth rate $\sigma$ (black) and potential energy density of the bedforms $E_z$ (blue) for the reference time-invariant simulation (thick solid line), $\theta = 2°$ (thin solid line), and $\theta = 4°$ (thin dotted line).

[22] Importantly, splittings are observed for only one of our time-invariant simulations for $H_s = 1.2$ m at about $t = 7$ days at $x = 2700$ m and 4300 m (Figure 5b). This is actually not the splitting of a rip channel into two rip channels but the splitting of a shoal (the shallowest section of the sandbar) through the formation of a rip channel in its center. Note that the two rip channels emerging from splitting at $t \approx 7$ days in Figure 5b subsequently merge to another rip channel. The development of channels in the center of a shoal will be referred to as a splitting in the following and will be discussed later in the paper.

[23] In contrast with $H_s$ and $T_p$, $\theta$ is crucial to the formation and subsequent nonlinear evolution of rip channels. Figure 6 shows the rip channel formation and subsequent nonlinear evolution for two wave angles to the shore. The model shows that for $\theta = 2°$ and $\theta = 4°$ rip channels stabilize for $\lambda \approx 600$ m and 1000 m, respectively. These two simulations show that rip spacing increases with $\theta$. Mergings of rip channels are ubiquitous for the two simulations and splittings are nonexistent. Figure 6c additionally shows that

the typical equilibrium timescale increases with increasing wave obliquity. Our finding that both rip spacing and equilibrium time increase with increasing $\theta$ is in agreement with existing modeling studies [e.g., *Deigaard et al.*, 1999; *Calvete et al.*, 2005; *Garnier et al.*, 2008].

## 4. Time-Varying Forcing Simulations

### 4.1. Wave Height and Period

[24] Consistent with the main time-invariant forcing results synthesized in the previous section, time-varying $H_s$ and $T_p$ had a limited influence on the evolution of rip channels. Therefore below we only show simulations with different values of the amplitude $A$ of sine wave time-varying $H_s$ and $T_p$ and the influence of the shape and period $T$ of the time-varying forcing is not addressed. Figure 7 shows the influence of the amplitude $A$ of $H_s$ variations on the evolution of rip channels for sine wave time-varying $H_s$ with a mean of 1 m (Figure 7a). The time evolution of the alongshore profile $Z_f$ $(x,100,t)$ for time-varying $H_s$ starting at $t = 4$ days is shown with $A = 0.1$ m (Figure 7b) and $A = 0.2$ m (Figure 7c). Results show that final mean rip spacing is the same as for the time-invariant forcing (Figure 4a) for both $A = 0.1$ and 0.2 m. Three-dimensional patterns systematically decay and grow during periods of low and high $H_s$ values, respectively. Overall, beach three-dimensionality decreases with increasing amplitude of $H_s$ variations (Figure 7d).

[25] The same applies for the influence of the time-varying $T_p$ simulations with a mean of 10 s (Figure 8). The time evolution of the alongshore profile $Z_f$ $(x,100,t)$ is shown for time-varying $T_p$ starting at $t = 4$ days (Figure 8a) with $A = 2$ s (Figure 8b) and $A = 4$ s (Figure 8c). Results are essentially similar to those with time-varying $H_s$, because both final rip spacing is the same as for the time-invariant reference simulation (Figure 4a) and beach three-dimensionality decreases with increasing $A$ (Figure 8d). Note that for the range of $H_s$ and $T_p$ values tested in this study, rip channels more rapidly respond to changes in $T_p$ than to changes in $H_s$ (e.g., larger $\sigma$ values in Figure 8e with respect to Figure 7e). Overall, the simulations show that both time-varying $H_s$ and $T_p$ have a negligible influence on mean rip spacing and that rip channels are systematically less developed for the time-varying simulations than for the time-invariant simulation. Similar results were obtained for different $T$ and shapes.

### 4.2. Wave Angle

[26] Below we address the impact of periodic time-varying $\theta$ with the influence of the amplitude $A$, the period $T$ and the shape of $\theta$ variations.

#### 4.2.1. Influence of the Amplitude $A$ of $\theta$ Time Evolution

[27] Figure 9 shows the influence of $A$ on the evolution of rip channels for sine wave time-varying, zero-mean $\theta$, with a period $T = 4$ days, $H_s = 1$ m and $T_p = 10$ s starting at $t = 4$ days. The time evolution of the alongshore profile $Z_f$ $(x,100,t)$ is shown with $A = 2°$ (Figure 9a), $A = 4°$ (Figure 9b), $A = 6°$ (Figure 9c), and $A = 8°$ (Figure 9d). Results show that low $A$ values do not significantly affect rip channel behavior with only small alongshore migration of the rip channels (Figure 9a) and a with final rip channel configuration with $\lambda$ essentially similar to that with time-invariant forcing (compared to Figure 4a).
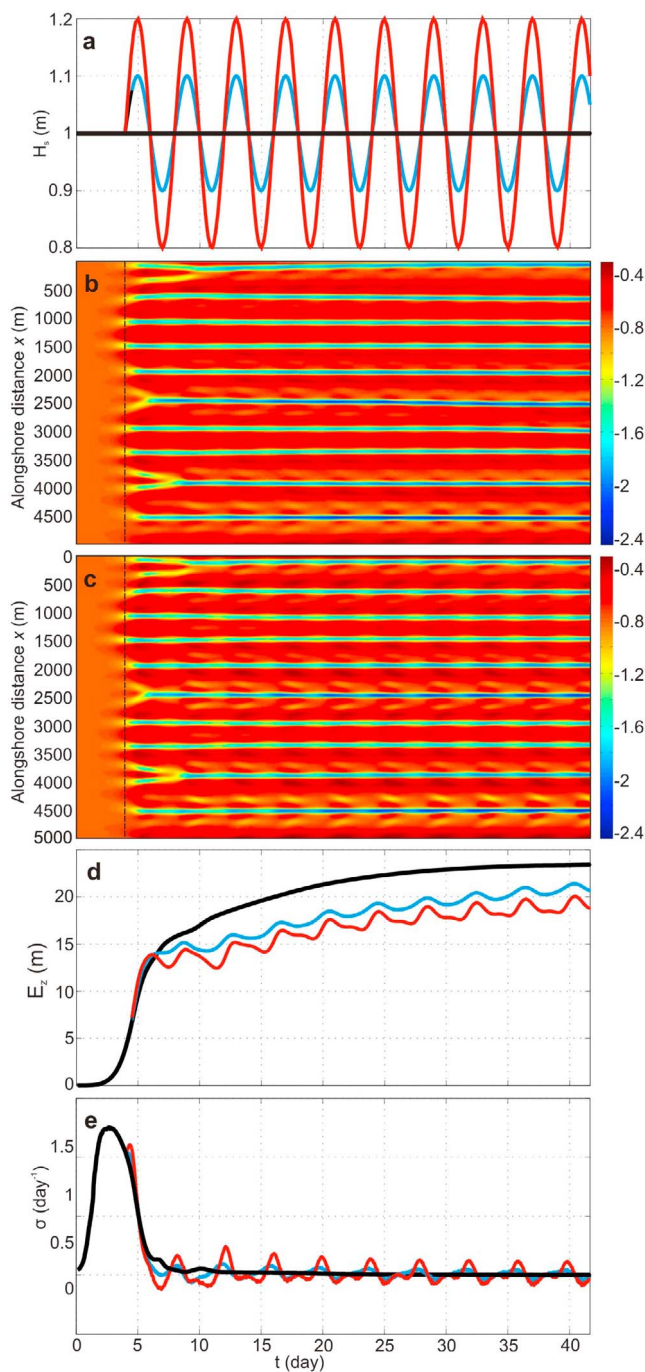
**Figure 7.** Influence on rip channel evolution of the amplitude $A$ of time-varying offshore significant wave height $H_s$ starting at $t = 4$ days, with a 1-m mean, a sine wave shape, $T = 4$ days, $\theta = 0°$, and $T_p = 10$ s. (a) Time series of $H_s$, (b, c) time evolution of the alongshore profile $Z_f(x,100,t)$ and corresponding time series of (d) potential energy density of bedforms $E_z$ and (e) global growth rate $\sigma$: $A = 0.1$ m (Figure 7b, in blue in Figures 7a, 7d, and 7e), $A = 0.2$ m (Figure 7c, in red in Figures 7a, 7d, and 7e). In Figures 7b and 7c the color bar indicates seabed elevation in meters and the vertical black dashed line indicates the start of time-varying $H_s$. In Figures 7a, 7d, and 7e the thick black line is the time-invariant simulation ($H_s = 1$ m).
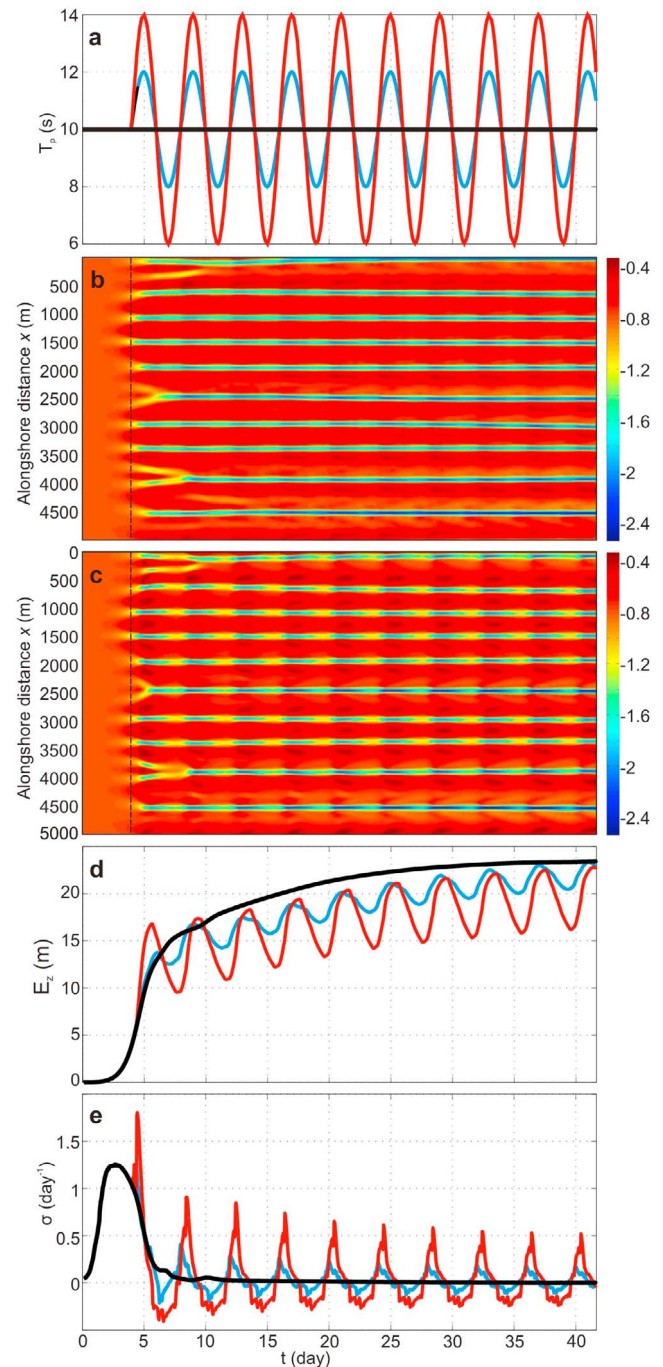
**Figure 8.** Influence on rip channel evolution of the amplitude $A$ of time-varying peak wave period $T_p$ starting at $t = 4$ days, with a 10-s mean, a sine wave shape, $T = 4$ days, $\theta = 0°$, and $H_s = 1$ m. (a) Time series of $T_p$, (b, c) time evolution of the alongshore profile $Z_f(x,100,t)$ and corresponding time series of (d) potential energy density of bedforms $E_z$, and (e) global growth rate $\sigma$: $A = 2$ s (Figure 8b, in blue in Figures 8a, 8d, and 8e), $A = 4$ s (Figure 8c, in red in Figures 8a, 8d, and 8e). In Figures 8b and 8c the color bar indicates seabed elevation in meters and the vertical black dashed line indicates the start of time-varying $T_p$. In Figures 8a, 8d, and 8e the thick black line is the time-invariant simulation ($T_p = 10$ s).
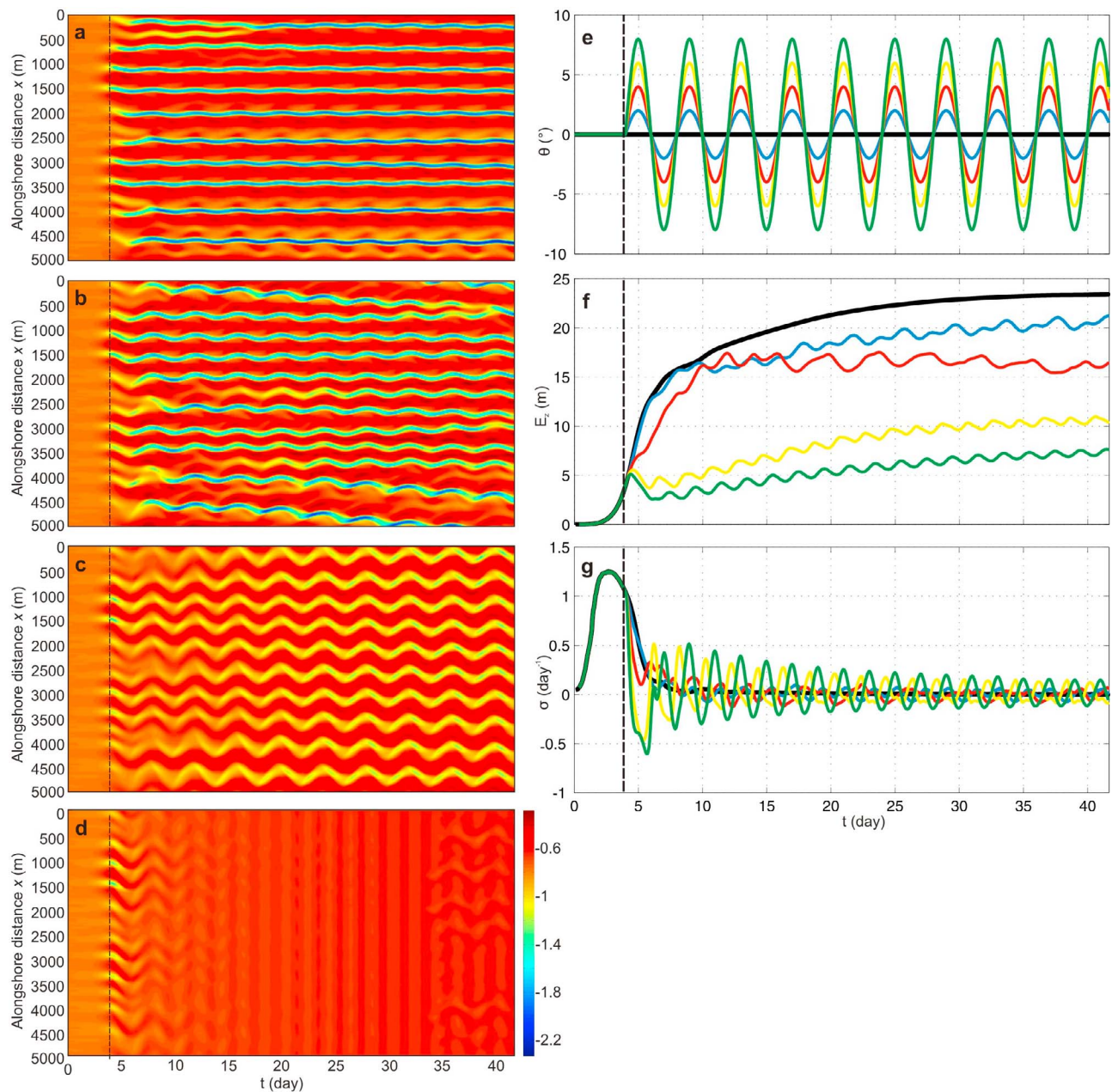
**Figure 9.** Influence on rip channel evolution of the amplitude $A$ of time-varying wave offshore wave angle to the shore $\theta$ starting at $t = 4$ days, with a 0-mean, a sine wave shape, $T = 4$ days, $H_s = 1$ m, and $T_p = 10$ s. (a–d) Time evolution of the alongshore profile $Z_f(x,100,t)$ and corresponding time series of (e) offshore wave angle to the shore $\theta$, (f) potential energy density of bedforms $E_z$, and (g) global growth rate $a$: $A = 2°$ (Figure 9a, in blue in Figures 9e–9g), $A = 4°$ (Figure 9b, in red in Figures 9e–9g), $A = 6°$ (Figure 9c, in yellow in Figures 9e–9g), $A = 8°$ (Figure 9d, in green in Figures 9e–9g). In Figures 9a–9d the color bar indicates seabed elevation in meters. In Figures 9a–9g the vertical black dashed line indicates the start of time-varying $\theta$. In Figures 9e–9g the thick black line is the time-invariant simulation ($\theta = 0°$).

[28] Increasing the amplitude in the $\theta$ variations to 4° increases the number of mergings with odd rapid alongshore migration of some rip channels (Figure 9b) as rip channels try to self-organize into more regular alongshore scales. Interestingly, splittings are observed about $t = 15$ days at $x = 2300$ m and 3700 m. The two rip channels that arise through splitting do not subsequently merge and have become two well-developed rip channels by the end of the simulation (Figure 9b). Despite rip spacing increasing with increasing $\theta$ in the time-invariant simulations, here rip spacing decreases with respect to the $\theta = 0°$ time-invariant simulation. For $A = 4°$ (Figure 9b), 11 to 12 rip channels are observed throughout the simulation (e.g., 12 rip channels for 15 days < $t$ < 27 days) instead of 10 in the time-invariant simulation (Figure 4a).
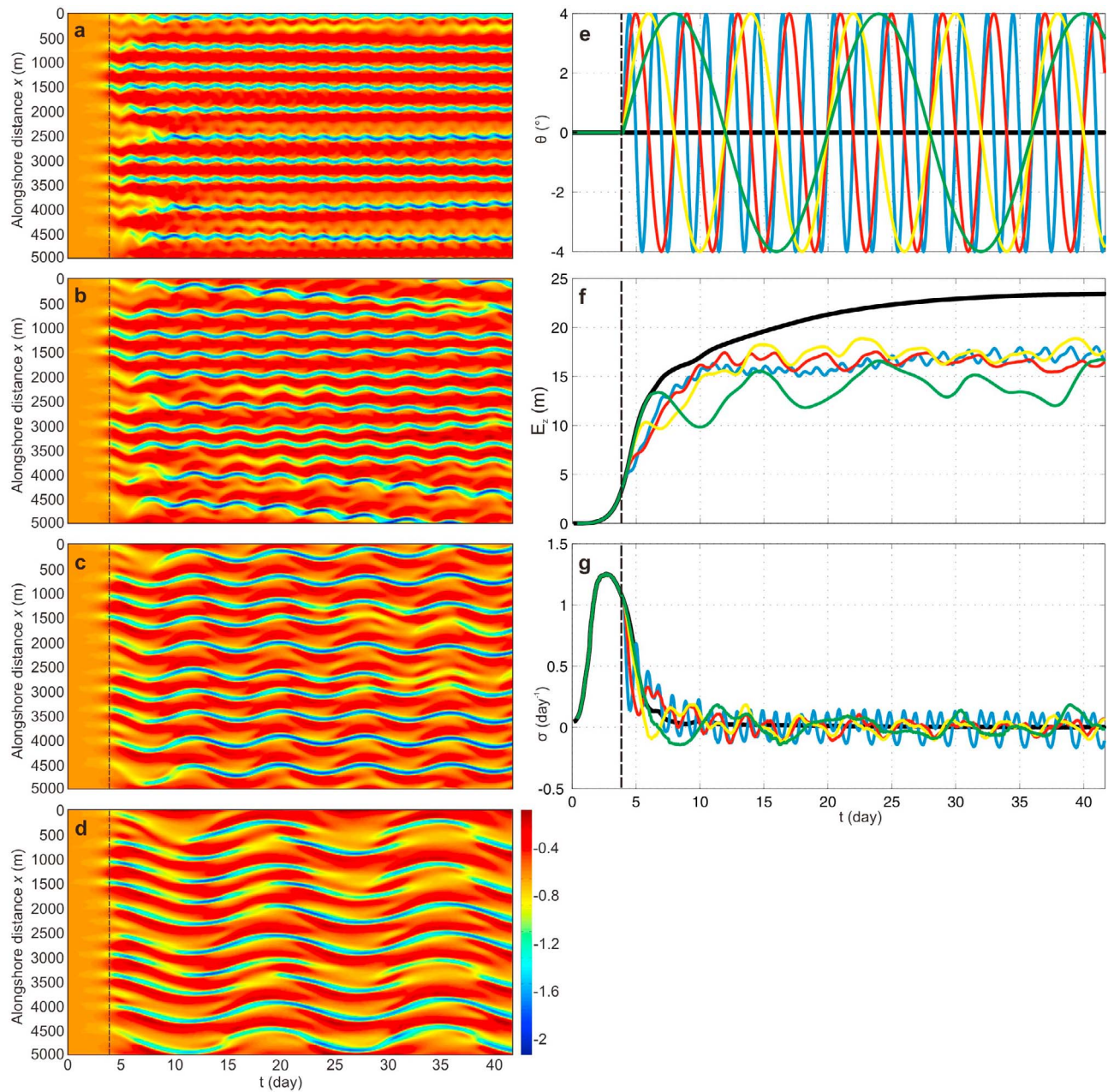
**Figure 10.** Influence on rip channel evolution of the period $T$ of time-varying offshore wave angle to the shore $\theta$ starting at $t = 4$ days, with a 0-mean, a sine wave shape, $A = 4°$, $H_s = 1$ m, and $T_p = 10$ s. (a–d) Time evolution of the alongshore profile $Z_f(x,100,t)$ and corresponding time series of (e) offshore wave angle to the shore $\theta$, (f) potential energy density of bedforms $E_z$, and (g) global growth rate $\sigma$: $T = 2$ days (Figure 10a, in blue in Figures 10e–10g), $T = 4$ days (Figure 10b, in red in Figures 10e–10g), $T = 8$ days (Figure 10c, in yellow in Figures 10e–10g), $T = 16$ days (Figure 10d, in green in Figures 10e–10g). In Figures 10a–10d the colormbar indicates seabed elevation in meters. In Figures 10a–10g the vertical black dashed line indicates the start of time-varying $\theta$. In Figures 10e–10g the thick black line is the time-invariant simulation ($\theta = 0°$).

[29] Further increasing $A$ to $6°$ drastically prevents mergings and splittings (Figure 9c) with a final rip spacing similar to that of the $\theta = 0°$ time-invariant simulation. Finally, higher $A$ values result in a progressive bar straightening at the beginning of the simulation (4 days $< t < 10$ days) driven by a strong longshore current ($\approx 0.8$ m/s) when $|\theta|$ temporarily exceeds about $6°$ during a sufficient duration

($\approx 1$ day). Overall, beach three-dimensionality decreases with increasing $A$ (Figure 9f) and increasingly keeps the morphology away from equilibrium (Figure 9g).

### 4.2.2. Influence of the Period $T$ of $\theta$ Time Evolution

[30] Figure 10 shows the influence of $T$ on the evolution of rip channels for sine wave time-varying $\theta$ with an amplitude

$A = 4°$, $H_s = 1$ m, and $T_p = 10$ s. The time evolution of the alongshore profile $Z_f(x,100,t)$ for time-varying $\theta$ starting at $t = 4$ days is shown for $T = 2$ days (Figure 10a), $T = 4$ days (Figure 10b), $T = 8$ days (Figure 10c), and $T = 16$ days (Figure 10d). The results show that for $T = 2$ days the rip channels are not significantly affected by the time-varying $\theta$ as they seem not to be able to adapt to the persistent rapid changes in $\theta$ (Figure 10a). This results in a final rip channel configuration and $\lambda$ that are essentially similar to those with time-invariant forcing. This agrees with *Smit et al.* [2005].

[31] For higher values of $T$ rip channels have more time to adapt to the changes in $\theta$. Rip channels and shoals therefore merge and split more frequently, respectively, which results in smaller rip spacing for $T = 4$ days (Figure 10b). Further increasing $T$ (Figures 10c–10d) results in a rather complicated behavior. For instance, for $T = 16$ days mergings and/or formations of rip channels become increasingly complex to discriminate from the quasiperiodic deepening and filling of rip channels (Figure 10d). Splittings are observed but rip channels subsequently merge rapidly or remain reasonably shallow throughout the simulation. Overall, changes in $T$ do not have any significant influence on beach three-dimensionality and all these simulations result in less-developed bar and rip morphologies compared to time-invariant $\theta = 0°$ forcing (Figure 10f). In addition, for $T = 2, 4$, and 8 days, 10 to 13 rip channels are observed throughout the simulations (Figures 10a, 10b, and 10c) which results in a generally smaller mean rip spacing than for the time-invariant simulation. The situation for $T = 16$ days is different because, as a result of the more slowly varying $\theta$, rip channels have more time to adapt to wave conditions which results in a situation that gets closer to the time-invariant forcing with oblique waves, i.e., with a larger mean rip spacing. Alongshore variability in rip channel depth and morphology is also found to increase with increasing $T$. In contrast, $T$ has a limited influence on the evolution of the global growth rate $\sigma$ (Figure 10g).

### 4.2.3. Influence of the Shape of $\theta$ Time Evolution

[32] Figure 11 shows the influence of the shape on the evolution of rip channel for time-varying $\theta$, with $T = 4$ days, $A = 4°$, $H_s = 1$ m, and $T_p = 10$ s. Four shapes are addressed: sine wave (Figure 11a), sawtooth (Figure 11b), sawtooth-sine wave (Figure 11c), and block function (Figure 11d), all with a zero mean $\theta$. A number of important results arise from these simulations.

[33] 1. The global growth rate decreases with increasing abruptness in $\theta$ variations. If the model is run for sufficient duration the $\theta$ shape does not have a significant influence on the, in quasi-equilibrium, beach three-dimensionality (Figure 11f).

[34] 2. In all these simulations with the same $T$ and $A$, rip spacing is generally smaller (10 to 13 rip channels, Figures 11a–11d) than that with $\theta = 0°$ time-invariant forcing (10 rip channels, Figure 4a).

[35] 3. Splittings are observed for the four situations, with for instance four to five splittings for the sawtooth-sine wave forcing in Figure 11c. The only exception is for the block function forcing for which only one splitting is observed at the end of the simulation at $x \approx 2700$ m (Figure 11d).

[36] 4. Surprisingly, when the time variation is asymmetric (sawtooth and sawtooth-sine wave), a strong net ($T$-averaged) alongshore migration of rip channels is observed (Figures 11b and 11c), despite a zero-mean $\theta$.

## 5. Discussion and Conclusions

[37] In this paper we investigated whether the nonlinear evolution of rip channels is influenced by time-varying wave height, period, and angle of incidence. Considering time-invariant forcing for a given basic state, $H_s$ and $T_p$ were found to have a significant influence on global growth rate and beach three-dimensionality as both $\sigma$ and $E_z$ typically increase with increasing $T_p$ and $H_s$ in the range of values tested in this study. This agrees with earlier linear or nonlinear stability analyses [e.g., *Calvete et al.*, 2005; *Garnier et al.*, 2008] that showed that the conditions most prone to rip channel formation occur for large wave height, long wave period, and normal incidence. In addition, $H_s$ does not have any significant influence on mean rip spacing as a result of a saturated basic state, which once again corroborates an earlier study [*Calvete et al.*, 2005]. In this paper our model was used for the first time to address long-term rip channel behavior. Overall, all our time-invariant forcing results agree with existing, time-invariant, modeling studies [e.g., *Deigaard et al.*, 1999; *Calvete et al.*, 2005; *Garnier et al.*, 2008], which supports the use of this numerical model to subsequently address the impact of time-varying wave forcing.

[38] The tuning parameters $\alpha$ and $\gamma$ in equation (3) were set to a small number of time-invariant simulations to have saturation of rip channels for the range of wave conditions used in this study. Using these parameters for time-varying forcing showed a systematic dynamic equilibrium of rip channels. While the effect of time-varying wave height and period was limited (in the range of conditions tested here), the influence of a time-varying angle of incidence was profound. Rip channels behave similarly (same rip spacing) to time-invariant forcing with $\theta = 0°$ only when the amplitude A and/or the period T of variation was very small, except that the final potential energy density of the bedforms was systematically lower than that for time-invariant forcing. Increasing $A$ or $T$ resulted in more complex behavior throughout the simulation. While rip spacing increases with increasing $\theta$ in time-invariant simulations, mean rip spacing decreases with increasing $\theta$ variability. The alongshore variability in rip channel depth and alongshore scales is also found to increase with increasing $\theta$ variability. This supports the common field observation of irregular and random spacing of rips alongshore [e.g., *Van Enckevort et al.*, 2004; *Turner et al.*, 2007] that is inconsistent with the regular spacing of rips alongshore predicted by existing, time-invariant, template, and instability models. Further increasing $A$ results in a progressive damping of the bed instability as rip channels become both increasingly obliquely oriented and decreasingly three-dimensional. This is similar to the development of the erosive transverse bar and rip state (eTBR) described by *Price and Ruessink* [2011].

[39] Time-varying wave incidence also generally resulted in the onset of splittings. In our simulations, we did not observe the splitting of the rip channel (i.e., bay) into two rip channels but the splitting of a shoal (the shallowest section of the sandbar) through the formation of a rip channel in its center. The only detailed field study of splittings deals with
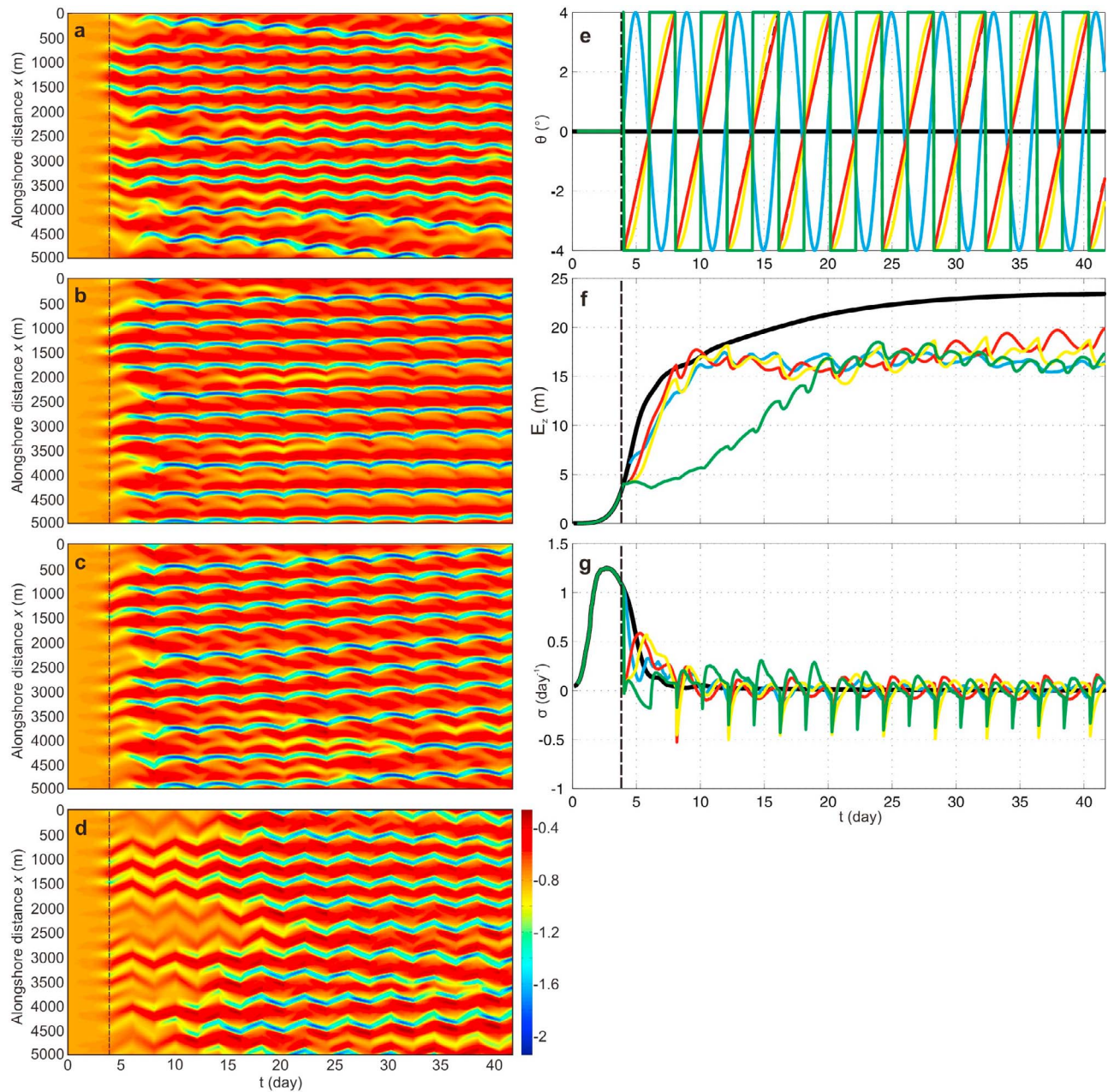
**Figure 11.** Influence on rip channel evolution of the shape of time-varying offshore wave angle to the shore $\theta$ starting at $t = 4$ days, with a 0-mean, a sine wave shape, $A = 4°$, $H_s = 1$ m, and $T_p = 10$ s. (a–d) Time evolution of the alongshore profile $Z_f(x, 100, t)$ and corresponding time series of (e) offshore wave angle to the shore $\theta$, (f) potential energy density of bedforms $E_z$, and (g) global growth rate $\sigma$: sine wave (Figure 11a, in blue in Figures 11e–11g), sawtooth (Figure 11b, in red in Figures 11e–11g), sawtooth-sine wave (Figure 11c, in yellow in Figures 11e–11g), block function (Figure 11d, in green in Figures 11e–11g). In Figures 11a–11d the color bar indicates seabed elevation in meters. In Figures 11a–11g) the vertical black dashed line indicates the start of time-varying $\theta$. In Figures 11e–11g the thick black line is time-invariant simulation ($\theta = 0°$).

crescentic sandbars [*Van Enckevort et al.*, 2004]. In their observations, splittings are characterized by the separation of a bay (seaward perturbation) into two crescentic patterns, that is, the other way around with respect to our simulations. However, despite not being focused on splittings, the time-evolution of the video-derived rip channel positions in the work of *Holman et al.* [2006] shows that splittings occur in

the same way as in our simulations. We noted that splittings were almost nonexistent in our time-invariant simulations. The same applies for existing time-invariant nonlinear morphodynamic modeling of rip channel evolution [e.g., *Garnier et al.*, 2008] in which, although sometimes claimed, there is no clear evidence of any splitting. Time-varying wave incidence generally resulted in the onset of splittings
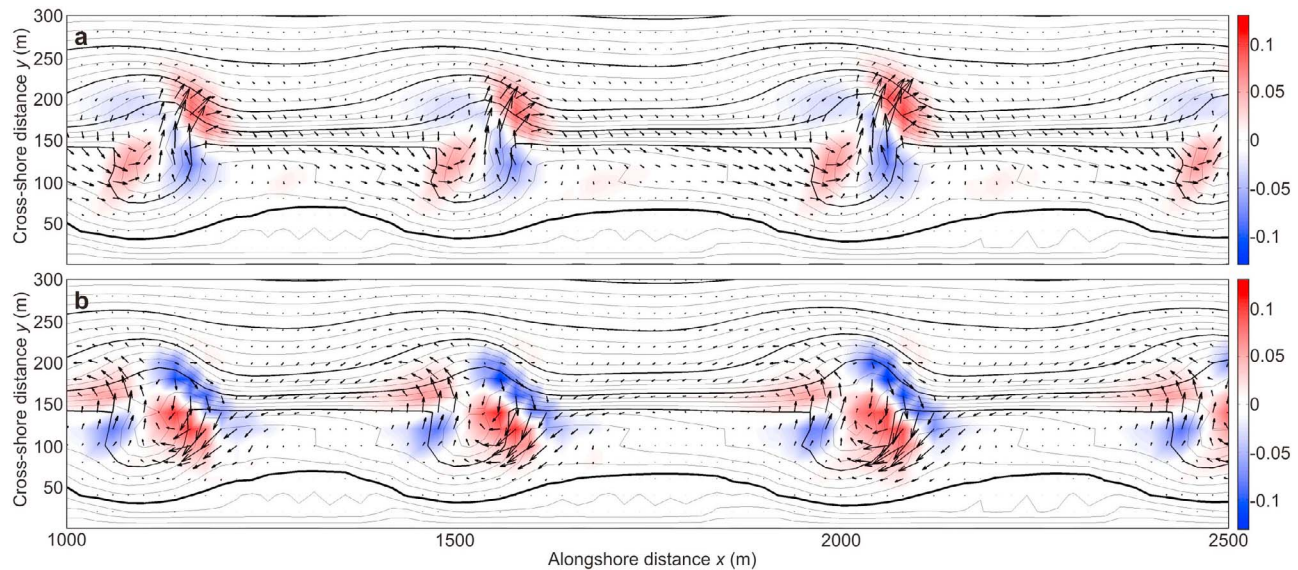
**Figure 12.** Zoom of the bathymetry at 1000 m < x < 2500 m and 0 m < y < 300 m with superimposed sediment transport field $\vec{Q}_s$ and resulting erosion $\partial Z/\partial t < 0$ (blue) and accretion $\partial Z/\partial t > 0$ (red) patterns for the sawtooth-sine wave time-varying wave angle (simulation in in Figure 11c) at $t \approx 36$ days (a) immediately before the abrupt change with $\theta = 4°$ and (b) immediately after with $\theta = -4°$. The local bottom morphology is contoured in the background and the color bars indicate $\partial Z/\partial t$ in meters per hour.

and an increased number of mergings. This agrees with *Van Enckevort et al.* [2004] who suggested that splittings and mergings are related to time-variations in the forcing. Our simulations are supported by additional field evidence: in our simulations, mergings and splittings are an attempt of the rip channels to self-organize into a more alongshore-uniform pattern as splitting is confined to the longest shoals, whereas merging usually combines the smaller rip spacings into a longer shoal (e.g., Figures 11a–11d). Only rarely did the rip channels arising through splittings develop into channels with a water depth similar to that of the other existing channels (e.g., Figure 11a). Most of the time rip channels arising through splittings remained reasonably shallow and subsequently (typically after 10–20 d) merged with another rip channel (e.g., Figures 11b and 11c).

[40] When $\theta$ variability is asymmetric (sawtooth and sawtooth-sine waves), the net ($T$-averaged) alongshore migration can be non-zero despite zero-mean $\theta$ (Figures 11b and 11c). As shown in Figure 11, all abrupt changes are characterized by a rapid decrease in beach three-dimensionality (Figure 11f) and a negative global growth rate (Figure 11g), which is the result of a rapid decrease in rip channel depth (see for instance in Figure 11d after each abrupt change). This is further emphasized in Figure 12, which shows the sediment transport field and resulting erosion/accretion patterns immediately before the abrupt change at $t \approx 36$ days for $\theta = 4°$ (Figure 12a) and immediately after (Figure 12b), corresponding to the sawtooth-sine wave simulation given in Figure 11c. Before the abrupt change, rip channels are skewed downdrift as they progressively adapted to the increasingly oblique wave approach. As a result, wave conditions before the abrupt change match the bar and rip orientation which results in classical sediment transport and erosion/accretion patterns with erosion and accretion at the downdrift and updrift part of the rip channel, respectively,

and a reasonably small accretion of the bar (Figure 12a). This both drives an alongshore migration of the rip channel and maintains rip channel three-dimensionality. Immediately after the abrupt change in wave conditions, rip channels are skewed updrift. Wave conditions mismatch the rip channel morphology as the angle of wave approach (and resulting wave-driven rip current skewness) is not in accordance with the bar/rip orientation. As a result, there is a reversal in the roles of each patch of accretion and erosion together with an increase in intensity (Figure 12b) that drive a switch in the migration direction and an increase in rate, respectively. In addition, this drives a rapid decrease in rip channel depth (see the significant decrease of $E_z$ in Figure 11b after each abrupt change). Given that, for a given oblique incidence wave condition, rip channel alongshore migration rate decreases with increasing rip channel depth, rip channel migration is enhanced after each abrupt change. Therefore rip migration is larger after an abrupt change in wave angle than before an abrupt change which, all cumulative, results in a net long-shore migration of the rip channel system. The role of this mismatch between sandbar morphology and prevailing wave conditions has previously been discussed in terms of near-shore circulations [e.g., *Sonu*, 1972; *Masselink and Hegge*, 1995]. Here we show that this mismatch may lead to a rapid decrease in rip channel volume, which facilitates a strongly increased alongshore migration rate of the rip channel directly after an abrupt change in wave angle.

[41] Our results imply that using mean wave conditions (typically averaged over $O$(weeks)) can be misleading when investigating alongshore migration of rip channels. Mean wave conditions have often been used to understand surf-zone sandbar alongshore migration [e.g., *Lafon et al.*, 2005; *Sénéchal et al.*, 2009; *Orzech et al.*, 2010]. While this approach sometimes proved to be a success [e.g., *Ruessink et al.*, 2000; *Orzech et al.*, 2010], correlations were not

that high as events of odd migration rates were common. More frequently poor correlation is found when quantifying rip channel alongshore migration rates as a function of prevailing wave conditions. *Turner et al.* [2007] measured a large number of rip channel migrations along the Gold Coast. The authors even found that migrations did not always occur in the direction consistent with the prevailing offshore swell direction and resulting alongshore current. We suspect that when rip channels are sufficiently well-developed, abrupt changes in wave conditions (particularly wave angle to the shore), can drive contrasting net rip channel migration because of the cumulative effects of the mismatch between hydrodynamics and sandbar morphology.

[42] The present nonlinear modeling exercise relies on a number of simplifying assumptions. For instance, we neglected the wave groupscale forcing that is known to influence rip spacing [*Reniers et al.*, 2004] as well as the 3-D structure of wave-driven circulations that can become significant in rip current settings [e.g., *Haas and Svendsen*, 2002]. These assumptions are commonly used for modeling 3-D surfzone sandbar behavior [e.g., *Garnier et al.*, 2008; *Smit et al.*, 2008]. More importantly, there are two key assumptions that need to be discussed. Simulations (not presented herein) showed that changing the basic state drastically impacts rip channel characteristics with similar results as in the work of *Calvete et al.* [2007]. Therefore our statement that changes in $H_s$ do not impact on rip spacing in the model is likely not to be relevant for situations where rip channels form and evolve similarly or less rapidly than the rate at which the beach profile is changing, that is, for large-amplitude changes in offshore wave heights. Correspondingly, *Van Enckevort et al.* [2004] indicated that most merging and splitting events took place during a significant increase and decrease in wave height, which was not possible to test with our model. A second assumption in our modeling study is that changes in wave conditions systematically occur at $t = 4$ days, that is, with a preexisting (yet slightly developed) sequence of horns and bays superimposed to the bar. The motivation for this choice was that, when starting time-varying wave angle forcing from the alongshore-uniform geometry, the dynamic equilibrium of rip channels systematically started later, typically at about $t = 20$–$25$ days for the $4°$-amplitude simulations. For $A > 4°$, rips sometimes did not even have the time to saturate by the end of the 41.5 day simulation. Thus we started the time-varying conditions at $t = 4$ days to keep the computation cost reasonable and to be able to accurately address merging/splitting dynamics for a large range of $A$. These preexisting bedforms may have impacted the subsequent evolution of rip channels. *Tiessen* [2010]showed that the influence of preexisting bedforms was limited if the initial bedform amplitude was small, the final dominant rip spacing always close to the dominant rip spacing found by linear stability analysis (i.e., without preexisting bedforms). The additional simulations starting with time-varying forcing at different times showed similar rip channel behavior as in the simulations presented in this paper. Therefore we think that the weakly developed preexisting pattern at $t = 4$ days does not influence our study outcomes significantly.

[43] Despite the limitations of our modeling approach, our results imply that the use of wave-climate mean values can be potentially misleading when investigating alongshore migration of surfzone sandbars, mean rip spacing, and beach three-dimensionality, and that sandbar response becomes increasingly complex when conditions change abruptly. The present nonlinear morphodynamic model has never been validated with field data, so the threshold values in $A$ and $T$ are to be considered in a qualitative way. Given the recent advances in process knowledge and numerical techniques in the nonlinear modeling of 3-D surfzone sandbar patterns, so far with application to academic cases only, a new step will be to study the response of a real-time sandbar system to natural changes in wave regimes. To do so, a crucial step is starting from an accurate nearshore bathymetry. Both the recent development of data-assimilation techniques [e.g., *Van Dongeren et al.*, 2008] and improvements in the understanding of cross-shore sandbar behavior [e.g., *Ruessink et al.*, 2007b], that should eventually prevent using the basic state assumption, will facilitate the emergence of data model comparisons.

## References

Almar, R., B. Castelle, B. G. Ruessink, N. Sénéchal, P. Bonneton, and V. Marieu (2010), Two- and three-dimensional double-sandbar system behaviour under intense wave forcing and a meso-macro tidal range, *Cont. Shelf Res.*, *30*, 781–792.

Bailard, J. A. (1981), An energetics total load sediment transport model for a plane beach, *J. Geophys. Res.*, *86*(C11), 10,938–10,954.

Battjes, J. A. (1975), Modelling of turbulence in the surfzone, paper presented at Symposium on Modelling Techniques, Am. Soc. of Civ. Eng., Reston, Va.

Booij, N., R. C. Ris, and L. H. Holthuijsen (1999), A third-generation wave model for coastal regions: 1. Model description and validation, *J. Geophys. Res.*, *104*(C4), 7649–7666.

Bruneau, N., B. Castelle, P. Bonneton, R. Pedreros, R. Almar, N. Bonneton, P. Bretel, J. P. Parisot, and N. Sénéchal (2009), Field observations of an evolving rip current on a meso-macrotidal well-developed inner bar and rip morphology, *Cont. Shelf Res.*, *29*, 1650–1662.

Calvete, D., N. Dodd, A. Falqués, and S. M. Van Leeuwen (2005), Morphological development of rip channel systems: Normal and near-normal wave incidence, *J. Geophys. Res.*, *110*, C10006, doi:10.1029/2004JC002803.

Calvete, D., G. Coco, A. Falqués, and N. Dodd (2007), (Un)predictability in rip channel systems, *Geophys. Res. Lett.*, *34*, L05605, doi:10.1029/2006GL028162.

Castelle, B., P. Bonneton, and R. Butel (2006a), Modeling of crescentic pattern development of nearshore bars: Aquitanian Coast, France, *C. R. Geosci.*, *338*, 795–801.

Castelle, B., P. Bonneton, N. Sénéchal, H. Dupuis, R. Butel, and D. Michel (2006b), Dynamics of wave-induced currents over an alongshore non-uniform multiple-barred sandy beach on the Aquitanian Coast, France, *Cont. Shelf Res.*, *26*, 113–131.

Castelle, B., B. G. Ruessink, P. Bonneton, V. Marieu, N. Bruneau, and T. D. Price (2010a), Coupling mechanisms in double sandbar systems, Part 1: Patterns and physical explanation, *Earth Surf. Processes Landforms*, *35*, 476–486.

Castelle, B., B. G. Ruessink, P. Bonneton, V. Marieu, N. Bruneau, and T. D. Price (2010b), Coupling mechanisms in double sandbar systems, Part 2: impact on alongshore variability of inner-bar rip channels, *Earth Surf. Processes Landforms*, *35*, 771–781.

Castelle, B., et al. (2010c), Laboratory experiment on rip current circulations over a moveable bed: Drifter measurements, *J. Geophys. Res.*, *115*, C12008, doi:10.1029/2010JC006343.

Coco, G., and A. B. Murray (2007), Patterns in the sand: from forcing templates to self-organization, *Geomorphol.*, *91*, 271–290.

Damgaard, J., N. Dodd, L. Hall, and T. Chesher (2002), Morphodynamic modeling of rip channel growth, *Coastal Eng.*, *43*, 199–221.

Deigaard, R., N. Drønen, J. Fredsøe, J. H. Jensen, and M. P. Jørgensen (1999), A morphological stability analysis for a long straight barred coast, *Coastal Eng.*, *36*, 171–195.

Drønen, N., and R. Deigaard (2007), Quasi-three-dimensional modelling of the morphology of longshore bars, *Coastal Eng.*, *54*, 197–215.

Falqués, A., G. Coco, and D. A. Huntley (2000), A mechanism for the generation of wave-driven rhythmic patterns in the surf zone, *J. Geophys. Res.*, *105*(C10), 24,071–24,088.

Gallop, S. L., K. R. Bryan, G. Coco, and S. Stephens (2011), Storm-driven changes in rip-channel patterns on an embayed beach, *Geomorphol.*, *127*, 179–188.

Garnier, R., D. Calvete, A. Falqués, and M. Caballeria (2006), Generation and nonlinear evolution of shore-oblique/transverse sand bars, *J. Fluid Mech.*, *567*, 327–360.

Garnier, R., D. Calvete, A. Falqués, and N. Dodd (2008), Modelling the formation and the long-term behavior of rip channel systems from the deformation of a longshore bar, *J. Geophys. Res.*, *113*, C07053, doi:10.1029/2007JC004632.

Garnier, R., N. Dodd, A. Falqués, and D. Calvete (2010), Mechanisms controlling crescentic bar amplitude, *J. Geophys. Res.*, *115*, F02007, doi:10.1029/2009JF001407.

Haas, K. A., and I. A. Svendsen (2002), Laboratory measurements of the vertical structure of rip currents, *J. Geophys. Res.*, *107*(C5), 3047, doi:10.1029/2001JC000911.

Holman, R. A., G. Symonds, E. B. Thornton, and R. Ranasinghe (2006), Rip spacing and persistence on an embayed beach, *J. Geophys. Res.*, *111*, C01006, doi:10.1029/2005JC002965.

Huntley, D. A., and A. D. Short (1992), On the spacing between observed rip currents, *Coast. Eng.*, *17*, 211–225.

Klein, M. D., and H. M. Schuttelaars (2006), Morphodynamic evolution of double-barred beaches, *J. Geophys. Res.*, *111*, C06017, doi:10.1029/2005JC003155.

Lafon, V., H. Dupuis, R. Butel, B. Castelle, D. Michel, H. Howa, and D. De Melo Apoluceno (2005), Morphodynamics of nearshore rhythmic sandbars in a mixedenergy environment (SW France): II. Physical forcing analysis, *Estuarine Coastal Shelf Sci.*, *65*, 449–462.

Masselink, G., and B. Hegge (1995), Morphodynamics of meso- and macrotidal beaches: Examples from central Queensland, Australia, *Mar. Geol.*, *129*, 1–23.

Masselink, G., A. Kroon, and R. G. D. Davidson-Arnott (2006), Morphodynamics of intertidal bars in wave-dominated coastal settings—A review, *Geomorphol.*, *73*, 33–49.

Orzech, M. D., E. B. Thornton, J. H. MacMahan, W. C. O'Reilly, and T. P. Stanton (2010), Alongshore rip channel migration and sediment transport, *Mar. Geol.*, *271*, 278–291.

Pape, L., N. G. Plant, and B. G. Ruessink (2010), On cross-shore sandbar behavior and equilibrium states, *J. Geophys. Res.*, *115*, F03008, doi:10.1029/2009JF001501.

Phillips, O. M. (1977), *The Dynamics of the Upper Ocean*, Cambridge Univ. Press, Cambridge, U. K.

Price, T. D., and B. G. Ruessink (2011), State dynamics of a double sandbar system, *Cont. Shelf Res.*, *31*, 659–674.

Reniers, A. J. H. M., J. A. Roelvink, and E. B. Thornton (2004), Morphodynamic modeling of an embayed beach under wave group forcing, *J. Geophys. Res.*, *109*, C01030, doi:10.1029/2002JC001586.

Ribas, F., and A. Kroon (2007), Characteristics and dynamics of surfzone transverse finger bars, *J. Geophys. Res.*, *112*, F03028, doi:10.1029/2006JF000685.

Ruessink, B. G., I. M. J. Van Enckevort, K. S. Kingston, and M. A. Davidson (2000), Analysis of observed two- and three-dimensional nearshore bar behaviour, *Mar. Geol.*, *169*, 161–183.

Ruessink, B. G., G. Coco, R. Ranasinghe, and I. L. Turner (2007a), Coupled and noncoupled behavior of three-dimensional morphological patterns in a double sandbar system, *J. Geophys. Res.*, *112*, C07002, doi:10.1029/2006JC003799.

Ruessink, B. G., Y. Kuriyama, A. J. H. M. Reniers, and J. A. Roelvink (2007b), Modeling cross-shore sandbar behavior on the timescales of weeks, *J. Geophys. Res.*, *112*, F03010, doi:10.1029/2006JF000730.

Sénéchal, N., T. Gouriou, B. Castelle, J.-P. Parisot, S. Capo, S. Bujan, and H. Howa (2009), Morphodynamic response of a meso- to macro-tidal intermediate beach based on a long-term dataset, *Geomorphol.*, *107*, 263–274.

Smit, M. W. J., A. J. H. M. Reniers, and M. J. F. Stive (2005), Nearshore bar response to time-varying conditions, paper presented at Coastal Dynamics '05, Am. Soc. of Civ. Eng., New York.

Smit, M. W. J., A. J. H. M. Reniers, B. G. Ruessink, and J. A. Roelvink (2008), The morphological response of a nearshore double sandbar system to constant wave forcing, *Coast. Eng.*, *55*, 761–770.

Sonu, C. J. (1972), Field observation of nearshore circulation and meandering currents, *J. Geophys. Res.*, *77*, 3232–3247.

Tiessen, M. C. H. (2010), The influence of pre-existing bed-forms on the development of crescentic bed patterns, paper presented at Linear stability analysis in coastal morphodynamics: Essential or useless?, Tech. Univ. of Catelonia, Barcelona, Spain.

Tiessen, M. C. H., S. M. Van Leeuwen, D. Calvete, and N. Dodd (2010), Field test of a linear stability model for crescentic sandbar, *Coast. Eng.*, *57*, 41–51.

Turner, I. L., D. Whyte, B. G. Ruessink, and R. Ranasinghe (2007), Observations of rip spacing, persistence and mobility at a long, straight coastline, *Mar. Geol.*, *236*, 209–221.

Van Dongeren, A. R., N. G. Plant, A. B. Cohen, J. A. Roelvink, M. C. Haller, and P. Catalán (2008), Beach Wizard: Nearshore bathymetry estimation through assimilation of model computations and remote observations, *Coastal Eng.*, *55*, 1016–1027.

Van Enckevort, I. M. J., and B. G. Ruessink (2003), Video observation of nearshore bar behaviour. Part 2: alongshore non-uniformity variability, *Cont. Shelf Res.*, *23*, 513–532.

Van Enckevort, I. M. J., B. G. Ruessink, G. Coco, K. Susuki, I. L. Turner, N. G. Plant, and R. A. Holman (2004), Observations of nearshore crescentic sandbars, *J. Geophys. Res.*, *109*, C06028, doi:10.1029/2003JC002214.

Vis-Star, N., H. de Swart, and D. Calvete (2008), Patch behaviour and predictability properties of modelled finite-amplitude sand ridges on the inner shelf, *Nonlinear Proc. Geophys.*, *15*, 943–955.

Wright, L. D., and A. D. Short (1984), Morphodynamic variability of surf zones and beaches: A synthesis, *Mar. Geol.*, *56*, 93–118.

B. Castelle, CNRS, UMR 5805 EPOC, Université de Bordeaux, Avenue des Facultés, F-33405 Talence CEDEX, France. (b.castelle@epoc.u-bordeaux1.fr)

B. G. Ruessink, Department of Physical Geography, Faculty of Geosciences, Institute for Marine and Atmospheric Research, Utrecht University, NL-3508 Utrecht, Netherlands.